Materials Horizons

COMMUNICATION

View Article Online
View Journal

Check for updates

Cite this: DOI: 10.1039/d5mh00965k

Received 21st May 2025,
Accepted 10th June 2025

DOI: 10.1039/d5mh00965k

rsc.li/materials-horizons

CNFs/Al_2O_3–SiC SBD flexible e-skin to achieve dual function sensing of pressure and temperature

He Gong,[ab] Lingyun Ni,[a] Hang Zhu,[a] Hongli Chao,[a] Lan Luo,[a] Mengchao Chen,[a] JinFan Wei,[a] Tianli Hu,[ab] Ying Guo,[ab] Zhiqiang Cheng,[c] Ye Mu*[ab] and Xiuling Yu*[a]

Human skin has the complex function of sensing pressure, strain, friction, temperature, and humidity. Flexible electronic skin (e-skin) plays a key role in advancing intelligent human–computer interaction and wearable health monitoring devices. However, achieving effective integration of multifunctional sensors while minimizing potential interference between them is a significant challenge. In this paper, we use an improved electrostatic spinning layered integration process to fabricate a sandwich-structured CNFs/Al_2O_3–SiC SBD pressure–temperature dual-mode e-skin, in which the top and bottom layers are composed of the temperature-sensitive material SiC SBD, which also functions as capacitive electrodes, forming a capacitive pressure sensor together with the pressure-sensitive material CNFs/Al_2O_3 in the middle layer. The experimental results show that the e-skin exhibits good performance in pressure and temperature tests: the response/recovery time of the pressure sensor is 0.52 s/0.53 s in the pressure range of 0–5 kPa, and the sensitivity reaches 0.366 kPa^{-1} in the range of 0–10 kPa. In the range of 25–50 °C, the response/recovery time of the top layer temperature sensor is 5.12 s/8.97 s, and the sensitivity can reach −1.291 $°C^{-1}$. In the range of 25–50 °C, the response/recovery time of the bottom layer temperature sensor is 4.96 s/8.92 s, and the sensitivity can reach −1.614 $°C^{-1}$. In this study, the preparation of CNFs/Al_2O_3–SiC SBD pressure–temperature dual-mode e-skin is described, which has good repeatability and independent sensing characteristics, unaffected by interference from other conditions. In addition, its excellent flexibility allows it to accurately perceive human movements and physiological signals such as gesture recognition and breath monitoring, while also detecting the spatial distribution of external stimuli, showing widespread application potential in intelligent human–computer interaction and wearable health monitoring devices.

New concepts

This paper proposes an electrospinning-based hierarchical integration process to fabricate a dual-mode flexible wearable electronic skin with a sandwich structure, successfully achieving synergistic integration of pressure and temperature sensing. Through dual breakthroughs in material system and microstructure design, the device constructs a "temperature–pressure–temperature" hierarchical functional architecture. The top and bottom layers composed of a temperature-sensitive SiC SBD material serve as resistive temperature sensors while simultaneously functioning as capacitive electrodes, which together with the intermediate CNFs/Al_2O_3 pressure-sensitive layer form a capacitive pressure sensor. The structure–function integrated design resolves interference issues in multifunctional sensor integration, realizing independent and high-precision pressure/temperature sensing capabilities. It shows a wide range of application prospects in the fields of intelligent human–computer interaction and wearable health monitoring.

1. Introduction

Human skin is an integrated network system with a variety of sensors and plays a vital role in sensing environmental stimuli such as pressure and temperature. Recently, e-skin has been widely studied with the development of sensors, such as pressure sensors,[1,2] strain sensors,[3,4] temperature sensors,[5,6] humidity sensors,[7,8] and gas sensors.[9,10] The use of modern electronic technology to imitate these functional characteristics of reconstructed skin and the preparation of artificial e-skin will have a profound impact on artificial prostheses, medical treatment and robotics.[11] In human–computer interaction, health monitoring, environment and virtual reality, soft robotics and other fields, sensors with various functions and excellent performance are being developed, and have a wide range of application prospects.[12–14]

[a] College of Information Technology, Jilin Agricultural University, Changchun, 130118, China. E-mail: muye@jlau.deu.cn, yuxiuling@jlau.edu.cn
[b] Jilin Province Intelligent Environmental Engineering Research Center, Changchun, 130118, China
[c] College of Resources and Environment, Jilin Agricultural University, Changchun, 130118, China

The design of multifunctional e-skin follows two approaches: the direct integration of multiple sensors and the multifunctionalization of a single sensor. Direct integration can simplify the preparation method, but it presents challenges such as integration complexity and reliability. The multifunctionalization of a single sensor achieves multiple functions through material fusion, but the sensitivity characteristics of physical quantities may interfere with each other, limiting functional expansion and selective testing, thereby affecting its application in complex environments. Feng[15] designed a self-powered multifunctional e-skin system with pressure, temperature, underwater sensing, and photothermal heating characteristics based on carbon nanotube/polydimethylsiloxane (CNT/PDMS) as a multifunctional sensing layer and power cathode, with a wide sensing range, excellent pressure sensitivity, and ultra-long-term durability. Fastier-Wooller[16] prepared carbon nanotube (CNT) films and polyacrylonitrile (PAN) interlayers, integrating pressure and temperature dual-mode sensors, providing a new approach for the development of robotic e-skin. Yin[17] designed a flexible pressure–temperature dual-mode sensor by inserting graphene into a thermoplastic polyurethane/carbon nanofiber (TPU/CNF) sponge with a multilayer structure, with high pressure sensitivity and high temperature sensitivity.

Carbon nanofibers (CNFs) are a new type of carbon material, with excellent physical properties and chemical stability, featuring a large specific surface area, high mechanical strength and Young's modulus, as well as high electrical and thermal conductivity properties, often used as conductive materials in flexible sensors. Adding metal ions to carbon nanofibers will greatly improve the resilience, sensitivity, responsiveness and other important characteristics of flexible sensors. Electrospinning is a low-cost, feasible and versatile technology, which can be used to produce fibers with nanometer diameters, high conductivities, high porosities, and low densities. This paper is based on an improved electrostatic spinning layered integration process, with carbon nanofibers as the research subject, and through doping and enhanced composite techniques, a sandwich-structured CNFs/Al_2O_3–SiC SBD pressure–temperature dual-mode e-skin was fabricated. The top and bottom layers are composed of the temperature-sensitive material SiC SBD, which also functions as capacitive electrodes, forming a capacitive pressure sensor together with the pressure-sensitive material CNFs/Al_2O_3 in the middle layer, and then the CNFs/Al_2O_3–SiC SBD dual-mode e-skin sensing properties were tested.

2. Experimental

2.1 Materials and methods

Polyacrylonitrile (PAN, molecular weight 15000) was obtained from Sinopharm Chemical Reagent Co., Ltd, dimethylformamide (DMF) from MACKLIN, silicic acid powder (H_2SiO_3) from Sinopharm Chemical Reagent Co., Ltd, and anhydrous aluminum chloride ($AlCl_3$) from Sinopharm Chemical Reagent Co., Ltd. All materials were used as received without any further processing.

2.2 Sensor fabrication

Prepare two solutions. In the first solution, dissolve 1.2 g PAN in 8.8 g DMF at 60 °C, stir at 150 r min^{-1} for 6 h, add 0.3 g $AlCl_3$ and stir for 4 h and stand for 24 h to obtain the pressure-sensitive spinning solution. In the second solution, dissolve 1.2 g PAN and 0.05 g H_2SiO_3 in 8.8 g DMF at 60 °C, stir at 150 r min^{-1} for 6 h, add 0.3 g $AlCl_3$ and stir for 4 h and stand for 24 h to obtain the temperature-sensitive spinning solution. This paper employs improved electrospinning apparatus featuring a dual-needle design. By switching between syringes, it is possible to fabricate multilayer flexible materials with adjustable layer thicknesses and independent structures using electrospinning technology. Two syringes were filled with temperature-sensitive spinning solution and pressure-sensitive spinning solution, respectively. Firstly, select the temperature-sensitive spinning solution, with a needle-to-collector distance of 180 mm, an applied voltage of 15 kV, a solution feed rate of 0.5 mL h^{-1}, and a rotational speed of 120 rad min^{-1}. Electrospinning was conducted for 2 h at 20 °C and 40% relative humidity to obtain a temperature-sensitive film material. Then, switch to the pressure-sensitive spinning solution, and adjust the distance to 200 mm. Electrospinning was performed for 4 h at 20 °C and 25% relative humidity, resulting in a temperature–pressure sensitive three-dimensional sponge material. Finally, switch back to the temperature-sensitive spinning solution, with the distance adjusted to 200 mm, and electrospun for 2 h at 20 °C and 40% relative humidity, thereby fabricating temperature–pressure–temperature sensitive nano-materials.

Place the materials in an electric oven, set the temperature to 60 °C and the time to 3 h for pre-oxidation, then set the temperature to 200 °C and the time to 2 h for further oxidation. During this process, the nanomaterials change from white to khaki. Finally, wait for the materials to cool down naturally. Preheat the tube furnace to 800 °C. Place the material in the tube furnace for 20 min to carbonize the bottom-layer temperature-sensitive material. Then, flip the material over and repeat the above steps to carbonize the top-layer temperature-sensitive material. Meanwhile, due to the relatively short carbonization time, the middle pressure-sensitive material remains un-carbonized. Finally, a sandwich-structured CNFs/Al_2O_3–SiC SBD pressure–temperature sensitive material is obtained. The top and bottom layers of the temperature sensitive material SiC SBD are the resistive temperature sensor and the capacitive electrode, and combined with the pressure-sensitive material CNFs/Al_2O_3 of the middle layer they form a capacitive pressure sensor. The CNFs/Al_2O_3–SiC SBD is cut into a regular shape with dimensions of 1 cm in length, 1 cm in width, and 0.5 cm in height. Subsequently, the material is encapsulated using a self-fabricated flexible fixture. The inner side of this flexible fixture is coated with a conductive layer. The upper and lower ends of the material are fixed to the flexible fixture with conductive silver paste. By means of the extended copper-foil electrodes, the changes in capacitance and resistance corresponding to pressure and temperature can be measured.

The experimental preparation process is shown in Fig. 1.

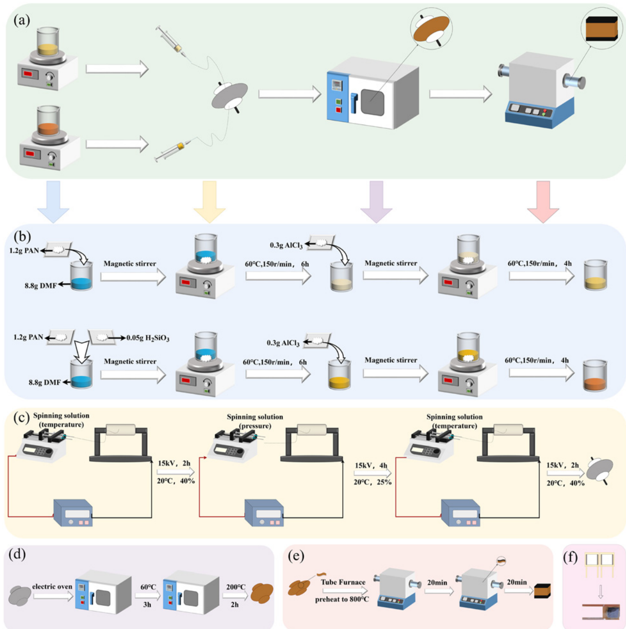

Fig. 1 Experimental process: (a) overall process of the experiment; (b) solution preparation; (c) electrospinning; (d) pre-oxidation; (e) carbonization; (f) encapsulation.

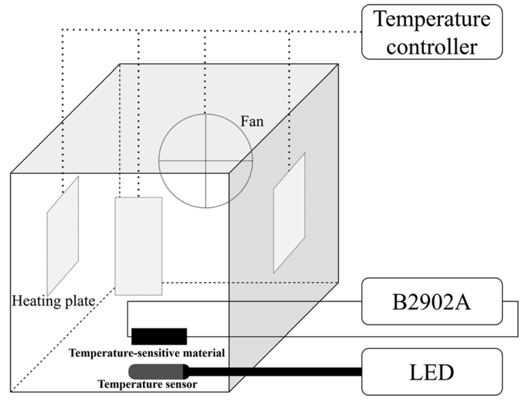

Fig. 2 Schematic diagram of the temperature testing device.

2.3 Characterization and performance measurements

The main equipment for material characterization testing includes: a scanning electron microscope (SEM), an energy dispersive X-ray spectrometer (EDS), model Shimadzux-550, an X-ray photoelectron spectrometer (XPS), model Nexsa XPS, and a Raman spectrometer, model Jobin Yvon Horiba T64000, with a light source wavelength of 532 nm.

The pressure performance testing system comprises an electronic universal testing machine and a digital source meter (KeithleyB2902A). Data collection and analysis are carried out using a computer. A voltage of 1 V is applied during the test. For the temperature performance test, a self-made temperature testing device is adopted as shown in Fig. 2. A thickened, sealed, and insulated acrylic component box with dimensions of 20 cm × 20 cm × 20 cm is selected. Inside the component box, a variable-power heating plate and a fan (used for heating and heat dissipation, with an external PWM temperature controller for temperature control), a high-precision digital-display temperature sensor (with an external LED to display the internal environmental temperature of the component box), and the sensor prepared in this paper (connected to a multi-channel digital source meter KeithleyB2902A for measuring the resistance of the temperature sensor) are added.

3. Results and discussion

3.1 Material characterization

Take the pressure-sensitive material CNFs/Al_2O_3 for characterization. Fig. 3(a) shows the electron microscopy scanning (SEM) image of the CNFs/Al_2O_3 material. At 1 μm magnification, the material fibers are stacked and intertwined with each other, and it can be seen that the fiber diameter uniformity is high and the surface is smooth, the average diameter of the nanofibers is 122.43 nm, the average breaking rate is 1.6%, the uniformity coefficient is 0.18%, and the number of beads is 2.0/100. Fig. 3(b) shows the energy dispersive spectroscopy (EDS) spectrum of the CNFs/Al_2O_3 material, which mainly contains C, O and Al, of which C accounts for 35%, O accounts for 20% and Al accounts for 10%. Fig. 3(c) shows the X-ray photoelectron spectroscopy (XPS) spectrum of the CNFs/Al_2O_3 material, and the carbon-containing functional groups in the material mainly include C–C (284.8 eV), C–O (286.67 eV) and C=O (288.61 eV). The corresponding contents were 69.72 at%, 18.78 at% and 11.5 at%. The oxygen element in the material mainly exists in three forms: Al_2O_3 (531.3 eV), C=O (532.61 eV) and C–O (533.92 eV), in which the content of Al_2O_3 is 17.47 at%, the content of the C=O functional group is 72.59 at%, and the content of the C–O functional group is 9.94 at%. There are two signal peaks for Al_4C_3 (73.13 eV) and Al_2O_3 (74.18 eV), and the corresponding contents are 35.55 at% and 64.45 at%.

Take the temperature-sensitive material SiC SBD for characterization. Fig. 4(a) shows the scanning electron microscopy (SEM) image of the SiC SBD material, the average diameter of the nanofibers is 120.42 nm, the average breaking rate is 2.7%, the uniformity coefficient is 0.17%, and the number of beads is 3.0/100. Fig. 4(b) shows the energy dispersive spectroscopy (EDS) image of the SiC SBD material, which mainly contains C, O, Al and Si, of which C accounts for 24%, O accounts for 9%, Al accounts for 21%

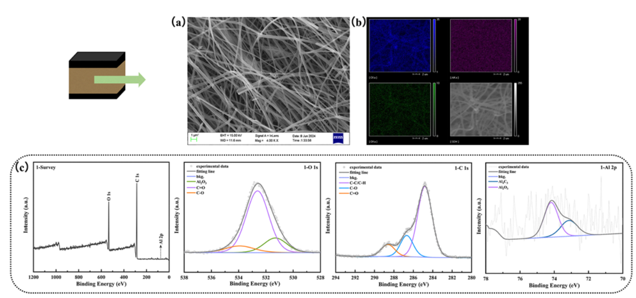

Fig. 3 Characterization tests of CNFs/Al_2O_3: (a) scanning electron microscopy (SEM); (b) energy dispersive spectroscopy (EDS); (c) X-ray photoelectron spectroscopy (XPS).

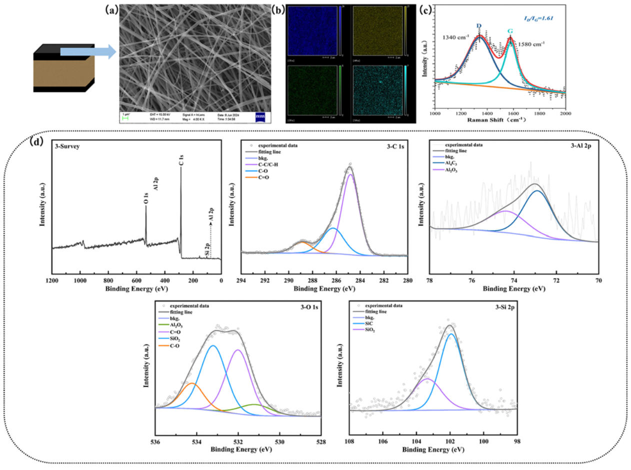

Fig. 4 Characterization tests of SiC SBD: (a) scanning electron microscopy (SEM); (b) energy dispersive spectroscopy (EDS); (c) Raman spectroscopy; (d) X-ray photoelectron spectroscopy (XPS).

and Si accounts for 7%. Fig. 4(c) shows the Raman spectrum of the SiC SBD material. There are two characteristic peaks belonging to the D-band and the G-band at approximately 1340 cm^{-1} and 1580 cm^{-1}. The appearance of the D-band and G-band reflects the existence of carbon structure in the material. The I_D/I_G value of the SiC SBD material is 1.61, indicating that the carbon phase introduced during the formation of SiC has a high defect level or low crystallinity. This structural feature may affect the carrier concentration and mobility of the material, and then affect its sensing characteristics as a resistance temperature sensor. Fig. 4(d) shows the X-ray photoelectron spectroscopy (XPS) test image of the SiC SBD material. In the material, there are obvious signal peaks of C element mainly at the three binding energy positions of 284.8 eV, 286.26 eV and 288.9 eV, corresponding to the C–C, C–O and C═O functional groups respectively, with contents of 64.42 at%, 25.7 at%, and 9.84 at%. The O element exists in the material in four forms: Al_2O_3 (531.17 eV), C═O (532 eV), SiO_2 (533.19 eV) and C–O (534.21 eV), with corresponding contents of 8.34 at%, 37.51 at%, 40.11 at%, and 14.05 at%. The Al elements in the material mainly exist in the form of Al_4C_3 (72.87 eV) and Al_2O_3 (74.33 eV), with corresponding contents of 61.87 at% and 38.13 at%. The fine spectrum analysis of Si elements shows that Si exists in the forms of SiC (101.92 eV, 65.95 at%) and SiO_2 (103.35 eV, 34.05 at%). Characterizations of the material's microstructure and chemical composition indicate that the SiC SBD composite has abundant carbon-phase defects, along with highly dispersed conductive and insulating phases. The temperature sensitivity is enhanced by constructing a multi-phase synergistic conductive network. Among them, SiC and Al_2O_3/SiO_2 jointly construct a high temperature stable structure, which effectively improves the thermal stability and temperature response of the material, and is suitable for the design and application of resistance temperature sensors in a wide temperature range.

3.2 Sensing test

In order to verify the pressure sensing characteristics of the CNFs/Al_2O_3–SiC SBD dual-mode e-skin prepared in this paper, we carried out a series of pressure tests. As shown in Fig. 5(a), in the pressure test of 5 kPa, the response time is 0.52 s and the recovery time is 0.53 s. As shown in Fig. 5(b), in 0–10 kPa pressure tests, the sensitivity can reach 0.366 kPa^{-1}, which is relatively higher than some other published pressure sensors[18–20] (as shown in Table 1). This shows that the pressure sensing of the CNFs/Al_2O_3–SiC SBD dual-mode e-skin prepared in this paper has a good response. In order to verify the temperature sensing characteristics of the CNFs/Al_2O_3–SiC SBD dual-mode e-skin prepared in this paper, we carried out a series of temperature tests. In the temperature test at 25–300 °C, both the top and bottom layer temperature sensors have good responses, as shown in Fig. 5(c), the response/recovery time of the top layer temperature sensor is 5.12 s/8.97 s, and as shown in Fig. 5(d), and the sensitivity can reach −1.291 $°C^{-1}$ in the range of 25–50 °C, −0.382 $°C^{-1}$ in the range of 50–100 °C, and −0.147 $°C^{-1}$ in the range of 100–300 °C. As shown in Fig. 5(e), the response/recovery time of the bottom layer temperature sensor is 4.96 s/8.92 s, and as shown in Fig. 5(f), the sensitivity can reach −1.614 $°C^{-1}$ in the range of 25–50 °C, the sensitivity can reach −0.382 $°C^{-1}$ in the range of 50–100 °C, and the sensitivity can reach −0.157 $°C^{-1}$ in the range of 100–300 °C. Relatively higher than some other published temperature

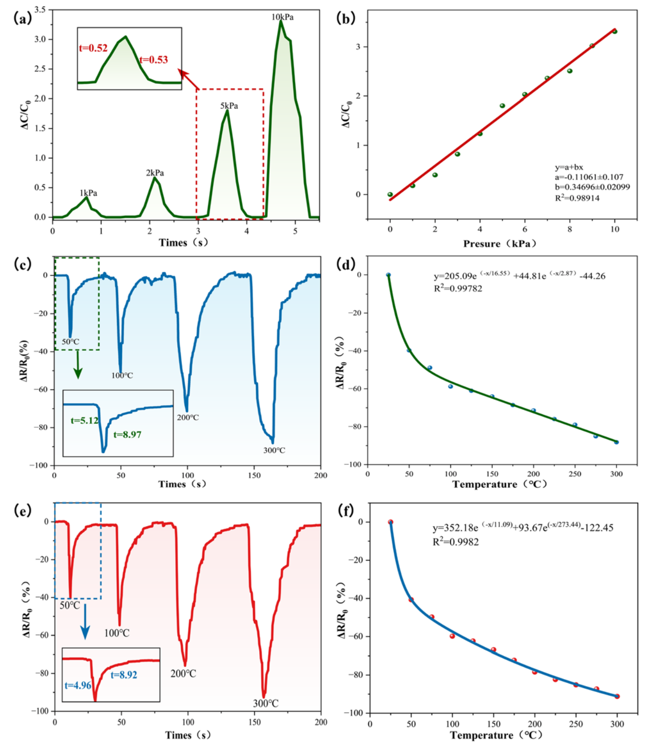

Fig. 5 Response test of the CNFs/Al_2O_3–SiC SBD dual-mode e-skin: (a) dynamic response of the pressure sensor's pressure–capacitance change rate; (b) pressure sensor's pressure–capacitance change rate fitting curve; (c) dynamic response of the temperature–resistance change rate of the top layer temperature sensor; (d) fitting curve of the temperature–resistance change rate of the top layer temperature sensor; (e) dynamic response of temperature–resistance change rate of the bottom layer temperature sensor; (f) fitting curve of the temperature–resistance change rate of the bottom layer temperature sensor.

Table 1 Sensitivity comparison of relevant pressure sensors

Material	Sensitivity (kPa^{-1})	Range (kPa)	Ref.
Parylene C/polyurethane	0.124	0.07–1.39	18
CuRGOMF	0.088	1.5–10	19
Silicon nanomembrane	0.0185	0–5	20
CNFs/Al_2O_3	0.366	0–10	This paper

sensors[21–23] (as shown in Table 2), it shows that the temperature sensing of the CNFs/Al_2O_3–SiC SBD dual-mode e-skin prepared in this paper has a good response. The impact of increasing temperature on the electrical conductivity of the material is closely related to the thermal excitation of covalent bonds. In materials with covalent bonds, such as those containing C–C or Si–C bonds, when the temperature rises, thermal excitation can cause the collapse of valence electron pairs.[24] When the temperature continues to rise and the breakage of covalent bonds reaches a saturated state, the increase in the number of free carriers generated by further temperature increase becomes smaller. This implies that the impact of temperature on electrical conductance weakens, the material's temperature response slows down, and correspondingly, the sensitivity of the temperature sensor decreases.[25]

Repeatability is an important index when measuring sensor performance, and the CNFs/Al_2O_3–SiC SBD dual-mode e-skin was tested repeatedly. As shown in Fig. 6(a) and (b), in the repeated pressure test, the test pressure is 1 kPa. In the repeated temperature test, the test temperature is 50 °C, and the repeated test for 2000 s is conducted. The repeated pressure test reaches ~1000 times and the repeated temperature test reaches ~50 times (because the temperature test environment needs time to adjust). The sensor still maintains good sensing performance, which proves that the CNFs/Al_2O_3–SiC SBD dual-mode electronic skin prepared in this paper has good repeatability and high stability. The environmental stability of the sensor is an important index to measure the performance, so the humidity sensitivity test of CNFs/Al_2O_3–SiC SBD dual-mode e-skin was tested, and the humidity range was 40–80%. As shown in Fig. 6(c) and (d), the test showed that the change of humidity had little influence on the pressure and temperature sensing characteristics of the dual-mode e-skin, and it had good environmental stability.

The multi-functional sensor should have a specific sensing ability, and react under specific conditions without interference from other sensing properties to ensure the reliability and accuracy of the application. Therefore, the CNFs/Al_2O_3–SiC SBD dual-mode e-skin prepared in this paper was tested for independent sensing characteristics. As shown in Fig. 7(a), the

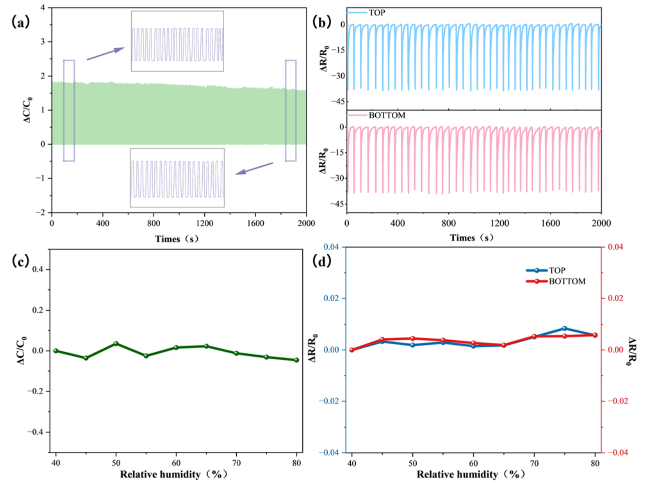

Fig. 6 Test of CNFs/Al_2O_3–SiC SBD dual-mode e-skin: (a) pressure repeatability test; (b) temperature repeatability test; (c) humidity response of the pressure sensor; (d) humidity response of the temperature sensor.

capacitance change rate of the pressure sensor was measured in the range of 20–60 °C. As shown in Fig. 7(b), the capacitance change rate of the pressure sensor was measured in the range of 0–10 kPa at room temperature and at 40 °C. The test shows that the sensing characteristics of the pressure sensor are not affected by temperature. The resistance change rate of the upper and lower temperature sensors is measured in the range of 0–10 kPa. As shown in Fig. 7(c), the test shows that the resistance change rate of the upper temperature sensor decreases slightly because the pressure is mainly applied to the upper temperature sensor, and as shown in Fig. 7(e), the resistance change rate of the lower temperature sensor is not much. The resistance change rate of the temperature sensor is measured under the conditions of no pressure and 5 kPa, and as shown in Fig. 7(d) and (f), the test shows that the sensing characteristics of the temperature sensor are basically not affected by pressure.

The CNFs/Al_2O_3–SiC SBD dual-mode e-skin was integrated into a 3 × 2 array, as shown in Fig. 8(a). A weight with a temperature of 50 °C and a weight of 50 g was placed on one end of the e-skin array, and the measured pressure distribution is shown in Fig. 8(b), since the flexible substrate has a certain elastic modulus, the pressure of adjacent units would change after the weight was added. The measured temperature distribution is shown in Fig. 8(c) and Fig. 8(d), the weight conducts heat to the adjacent unit, resulting in an increase in the temperature of the sensor unit without the weight added. It is proved that the pressure–temperature e-skin array can accurately reflect the distribution of pressure and temperature in practical applications.

Table 2 Sensitivity comparison of relevant temperature sensors

Material	Sensitivity	Range (°C)	Ref.
CNT/MXene	−0.52% $°C^{-1}$	−20 to 220	21
Ag based on fabric substrate	0.00262 $°C^{-1}$	25–42	22
rGO/LIG	0.0156 $°C^{-1}$	25–45	23
SiC SBD	−1.614 $°C^{-1}$	0–50	This paper

3.3 Sensing mechanism

This study employs an improved electrostatic spinning layered integration process to fabricate a sandwich-structured CNFs/Al_2O_3–SiC SBD pressure–temperature dual-mode e-skin, the top and bottom layers are composed of the temperature-sensitive

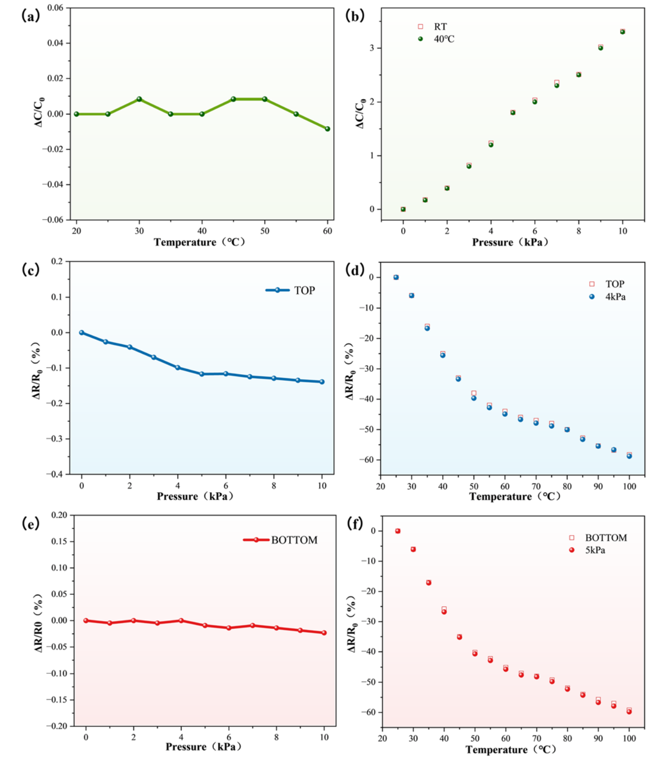

Fig. 7 Independent sensing characteristic test of CNFs/Al_2O_3–SiC SBD dual mode e-skin: (a) capacitance change rate of the pressure sensor in the range of 20–60 °C; (b) the capacitance change rate of the pressure sensor at 0–10 kPa at room temperature and at 40 °C; (c) the resistance change rate of the top layer temperature sensor in the range of 0–10 kPa; (d) resistance change rate of the top layer temperature sensor under no-pressure and 5 kPa conditions; (e) the resistance change rate of the bottom layer temperature sensor in the range of 0–10 kPa; (f) resistance change rate of the bottom layer temperature sensor under no-pressure and 5 kPa conditions.

material SiC SBD, which also functions as capacitive electrodes, forming a capacitive pressure sensor together with the pressure-sensitive material CNFs/Al_2O_3 in the middle layer. The electrospinning precursor solution plays a crucial role in the formation of the three-dimensional nanofiber sponge.[26] $AlCl_3$ serves as an aluminum-ion source (Al^{3+}) for constructing the three-dimensional nanofiber sponge.[27,28] Adding an appropriate amount of $AlCl_3$ to the PAN solution and thoroughly mixing it can increase the viscosity of the precursor solution,[29] then enhance the spinning ability of the precursor solution and the solidification rate of the fibers. In addition, during the electrospinning process, Al^{3+} is prone to being polarized under the effect of a strong electric field. As a result, the repulsive force between the charged Taylor cones/fibers increases. This also facilitates the solidification of the fibers, thus contributing to the formation of the three-dimensional nanofiber sponge. Then after a series of heat treatments $AlCl_3$ is converted to Al_2O_3, which is uniformly dispersed on the nanofibers, giving the material good support and mechanical properties.[30,31] Nanofibers with random multi-morphology and disordered multi-layer stacking form a large number of microstructures on the contact surface as shown in Fig. 9. When subjected to external pressure, the contact area of the sensor changes greatly, and the speed at which the microstructure deformation of the contact interface reaches saturation can be slowed down, which helps the flexible pressure sensor achieve higher sensitivity in a wide pressure range.[32] However, the multi-layer stacked structure,[33] cracked structure,[34] and porous structure[35] in the material further enhance the pressure-sensitive properties.

In the temperature sensor layer, SiC nanofibers are formed by the reaction of polyacrylonitrile (PAN) and H_2SiO_3 precursors at high temperature. Considering that PAN is a nitrogen-containing precursor, nitrogen may be partially incorporated into the SiC lattice during high-temperature carbonization, making SiC nanofibers exhibit n-type semiconductor properties. After high temperature treatment, the $AlCl_3$ precursor added in the experiment is expected to exist mainly in the form of Al_2O_3 second phase particles in or on the surface of SiC nanofibers. Carbon nanofibers have good conductivity, and their Fermi level is different from the conduction band formation energy band of this n-type SiC, so they can form a Schottky barrier diode (SBD) when they are in contact.

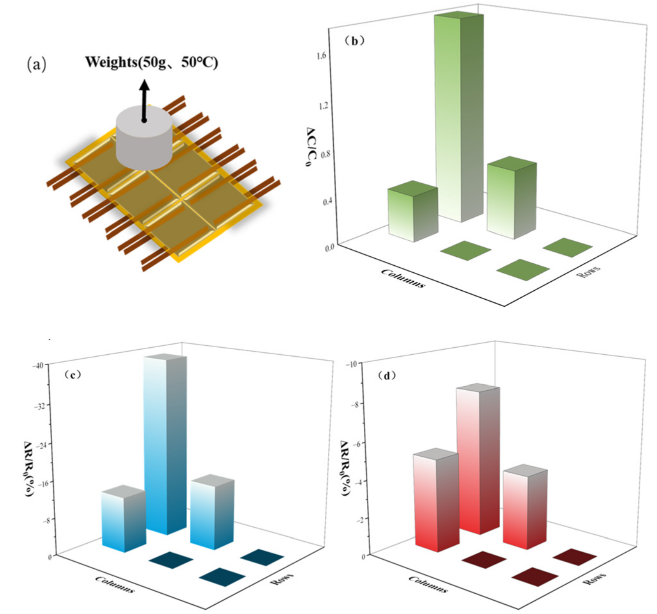

Fig. 8 CNFs/Al_2O_3–SiC SBD dual-mode e-skin array test: (a) E-skin array test diagram; (b) pressure distribution diagram; (c) top layer temperature distribution diagram; (d) bottom layer temperature distribution diagram.

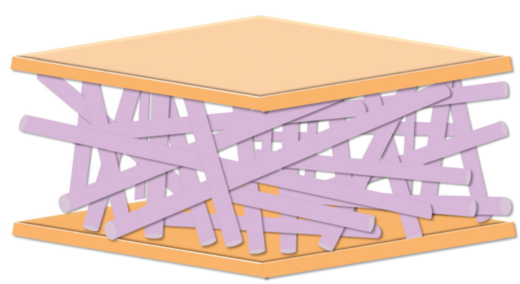

Fig. 9 Schematic of the material interior.

When SBD is in the constant current and effective temperature range, there is a linear relationship between the forward voltage drop and temperature change, demonstrating temperature sensitive characteristics. Due to the presence of a large number of SiC SBD structures within the prepared temperature-sensitive material, it exhibits good temperature-sensing performance. The current conduction mechanism of SiC SBD can be explained by the theory of hot electron emission,[36] as shown in eqn (1).

$$I = I_s \exp\left[\frac{q(V - IR_{on})}{nkT} - 1\right] \quad (1)$$

In the equation: $I_s = A \times A^* \times T^2 \times \exp\left(-\frac{q\varphi_B}{kT}\right)$, A is the Schottky contact area, A^* is the Richardson constant usually 120 A cm^{-1} 2k^{-2}, k is the Boltzmann constant, and φ_B is the height of the Schottky barrier diode; n is the ideal factor; V is the forward voltage drop; R_{on} is the series resistance. Eqn (1) is transformed to obtain eqn (2).

$$V = \frac{nkT}{q}\ln\frac{I}{AA^*T^2} + n\varphi_B + \mathrm{IR}_{on} \quad (2)$$

In the equation, $\ln\left(\frac{I}{AA^*T^2}\right)$ changes with temperature, but the amplitude of change is small, and the amplitude relative to temperature can be ignored, which is regarded as a constant. Since n, φ_B, and R_{on} all change with temperature, and R_{on} is affected by the positive conduction current, when the forward current is very small, R_{on} is very little affected by temperature.[37] φ_B is related to the surface state inside the material and the uneven distribution of the interface layer, and is less affected by the temperature change. In eqn (2), only the ideal factor n affects the sensitivity. As the temperature increases, the ideal factor n increases and the sensitivity decreases,[38] which can also explain why the sensitivity of the sensor begins to decline at 50 °C. The sensing material is formed by the braiding of multiple one-dimensional nanofibers, where the nanofibers are interleaved to form series, parallel, and bridge structures on the SBD of each nanofiber, and several connection modes of Schottky diodes can improve its temperature sensitivity.[39]

Based on the theoretical model of hot electron emission, the *I–V* characteristics of the top-layer temperature sensor were tested at different temperatures, as Fig. 10 shows. The actual Schottky barrier height φ_B = 0.65–0.72 eV, and the ideal factor n = 1.02–1.07 were calculated, which were consistent with the basic characteristics of typical Si based Schottky diodes (φ_B = 0.729–0.749 eV, n = 1.083–1.119),[40] verifying the accuracy of the model.

The flexible temperature–pressure sensor based on electrospinning technology achieves independent sensing functions through a layered design: the top and bottom layers consist of conductive temperature-sensitive materials used to measure temperature changes, with their resistance varying as the temperature rises or falls; the middle layer is composed of a non-conductive pressure-sensitive material, whose dielectric constant and thickness change under pressure, thereby affecting the capacitance between the top and bottom layers, which is used to measure pressure changes. Since the resistance is solely related to temperature and the capacitance is solely related to pressure, the two do not interfere with each other, as the changes in resistance and capacitance are driven by different physical mechanisms, as Fig. 11 shows. Additionally, the conductivity and microstructure of the materials were optimized through appropriate heat treatment, further ensuring the functional separation of the temperature-sensitive and pressure-sensitive materials. This guarantees that the sensor can independently and accurately detect temperature and pressure signals. The top and bottom layers of SiC SBD resistive temperature sensors are used as capacitive electrodes and intermediate layer pressure sensitive materials to form capacitive pressure sensors, and the structural design aims to realize the integration and versatility of the sensor. This design not only simplifies the structural design, but also exhibits excellent sensing performance. Although the resistance of the SiC SBD temperature-sensitive material is at the kΩ level, compared to the pressure-sensitive material with an insulating middle layer, the SiC SBD layer possesses relatively higher conductivity, and can effectively serve as a capacitor electrode. Importantly, for capacitive pressure sensors, the primary focus is on the relative change in capacitance caused by applied pressure, and this change can be clearly detected in experimental testing, which indicates that the resistance at the kΩ level does not impede the sensing function of the capacitive pressure sensor.

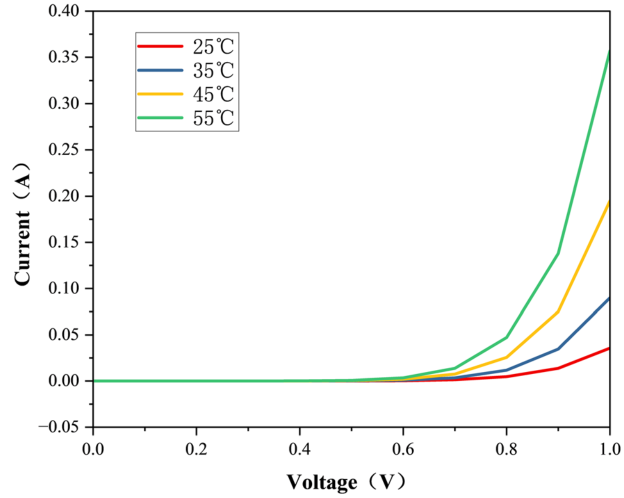

Fig. 10 *I–V* test curve.

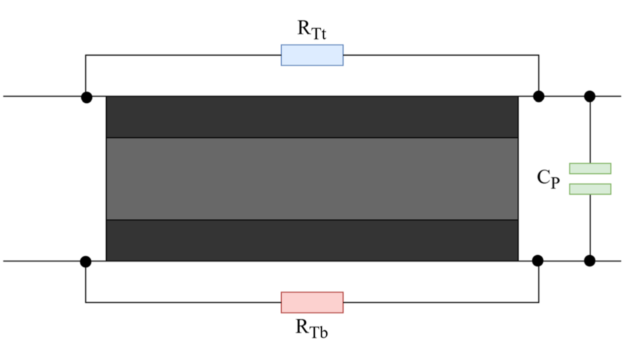

Fig. 11 Circuit schematic.

3.4 Applications

3.4.1 Application of e-skin sensors in hands. In order to explore the practical application effect of the CNFs/Al_2O_3–SiC SBD dual-mode e-skin, the pressure and temperature of the sensor are stimulated simultaneously by pressing the finger. The measured real-time response of the temperature signal and pressure signal of the e-skin sensor under finger pressure is shown in Fig. 12(a). The finger presses the e-skin with different forces, and the capacitive signal output by the pressure sensor follows the change in finger pressure in real time during this period. After four presses, the finger leaves the e-skin, and the output resistance of the top layer temperature sensor returns to the initial value. The CNFs/Al_2O_3–SiC SBD dual-mode e-skin was attached to the knuckle of the index finger. As the index finger bent to different degrees, the temperature signal and pressure signal are shown in Fig. 12(b). The greater the degree of bending, the higher the peak value of the pressure signal. Place the CNFs/Al_2O_3–SiC SBD dual-mode e-skin on the palm of the left hand for the clapping action, as shown in Fig. 12(c), when the two palms touch, the pressure signal reaches a distinct peak, indicating the moment of the clap action. During contact, the top layer temperature sensor senses the rise in the temperature of the right palm and the decrease in resistance, while the bottom layer temperature sensor detects the temperature of the left palm. The resistance does not decrease significantly during the clapping action, but there is a small fluctuation during the clapping action. Place the CNFs/Al_2O_3–SiC SBD dual-mode e-skin on the surface of the water cup, inject water with different volumes into the cup, place the hand at the position of the device, and observe the pressure and temperature signals when picking up the water cup, as shown in Fig. 12(d). The pressure signal felt by the e-skin will increase with the water capacity.

3.4.2 Application of e-skin sensing in gesture recognition. The e-skin sensor attached to the knuckle of the hand for a gesture recognition test can effectively monitor the joint pressure and deformation signals caused by different gestures to identify and distinguish specific gestures. In the test, the ''Stop'', ''Six'', ''Ok'' and ''Yeah'' gestures were detected. As shown in Fig. 13(a), the ''Stop'' gesture is displayed with the palm spread flat and the fingers fully extended. At this point, the sensor will detect a baseline signal of no significant bending at the knuckle of the hand. As shown in Fig. 13(b), the ''Six'' gesture is displayed with the pinky and thumb extended and the remaining fingers bent. The sensor will record no significant pressure changes in the pinky and thumb joints, while the other bent fingers will show higher pressure changes. As shown in Fig. 13(c), the ''OK'' gesture is represented by the thumb and index finger touching to form a ring, with the remaining three fingers extended. This gesture will produce a significant pressure signal at the index finger joint, while the thumb bend will also cause a response at the corresponding position of the sensor, and the rest of the fingers show no significant pressure signal. As shown in Fig. 13(d), the ''Yeah'' gesture is characterized by the extension of the index and middle fingers while the other fingers remain bent. The sensor detected no significant pressure signals on the extended index and middle fingers, while the remaining bent fingers recorded notable pressure changes.

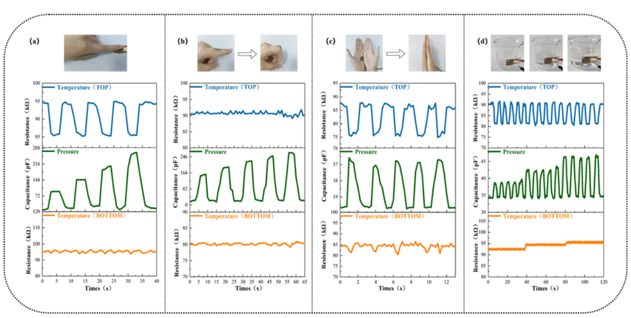

Fig. 12 Application of the e-skin sensor in hands: (a) finger press; (b) finger curvature; (c) clap hands; (d) holding cups of different capacities.

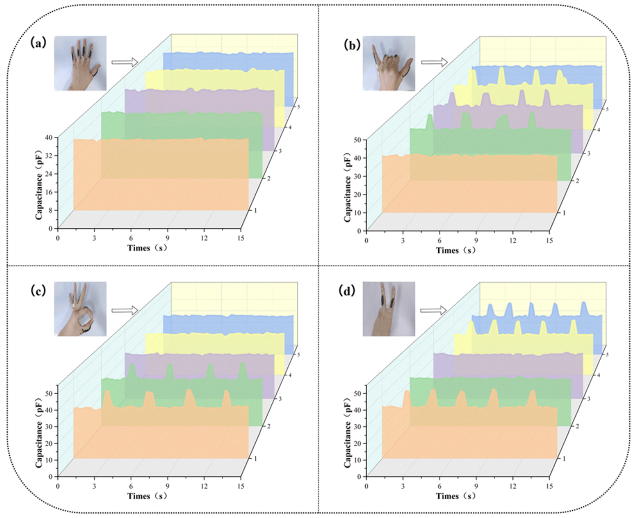

Fig. 13 Application of e-skin sensing in gesture recognition: (a) ''Stop''; (b) ''Six''; (c) ''Ok''; (d) ''Yeah''.

3.4.3 Application of the e-skin sensor in the throat. The e-skin sensor was attached to the throat joint, as shown in Fig. 14(a), to monitor the pressure changes of different movements. Four specific movements were recorded: nod, shake head, cough and swallow. The waveform of the sensor output signal is shown in Fig. 14(c)–(f). PCA (principal component analysis) is applied to the signals of these actions captured by the sensor. PCA is an unsupervised learning-based multivariate statistical analysis method that can efficiently identify the principal components in the data. As shown in Fig. 14(b), according to the results of PCA analysis, obvious clustering phenomenon was observed in the four action signals, indicating that different action pressure modes have significant distinguishability, and can be further used in pattern recognition systems to achieve real-time action recognition and classification through building classifiers or machine learning models. This has significant application value for the development of intelligent wearable devices and motion detection in human–computer interaction.

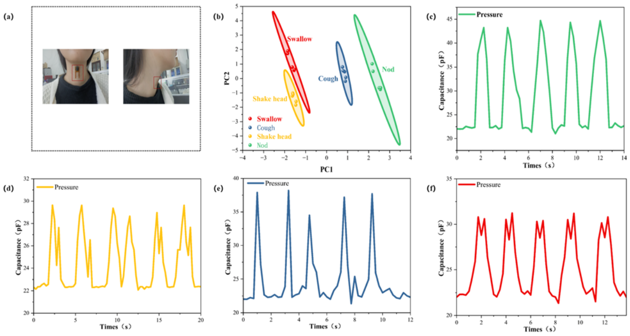

Fig. 14 Application of the e-skin sensor in the throat: (a) schematic diagram; (b) PCA analysis; (c) nod; (d) shake head; (e) cough; (f) swallow.

3.4.4 Application of the e-skin sensor in respiratory monitoring. In human respiration monitoring, the e-skin sensor shows an obvious response to changes in pressure and temperature. In the test, the sensor was attached to the mask, as shown in Fig. 15(b), to assess its ability to monitor different breathing patterns, including normal breathing, deep breathing, and mouth breathing. The sensing signals of the three respiratory behaviors are shown in Fig. 15(a), and the results show that the temperature–resistance and pressure–capacitance signals fluctuate synchronously with changes in the respiratory rate. As the number of breaths increases, the temperature inside the mask gradually increases, resulting in a slight overall decrease in the initial resistance of the sensor. The PCA analysis of these three breathing signals is shown in Fig. 15(c), and the results show that the sensor exhibits an obvious clustering phenomenon, which can effectively distinguish normal breathing, deep breathing, and mouth breathing. This indicates that the flexible dual-mode e-skin has a high discrimination ability in respiratory monitoring.

E-skin sensors are used in sleep breathing tests to monitor users' sleep breathing behavior and record sleep activities, such as apnea and nightmares. This enables users to assess their sleep status for potential health problems and seek timely

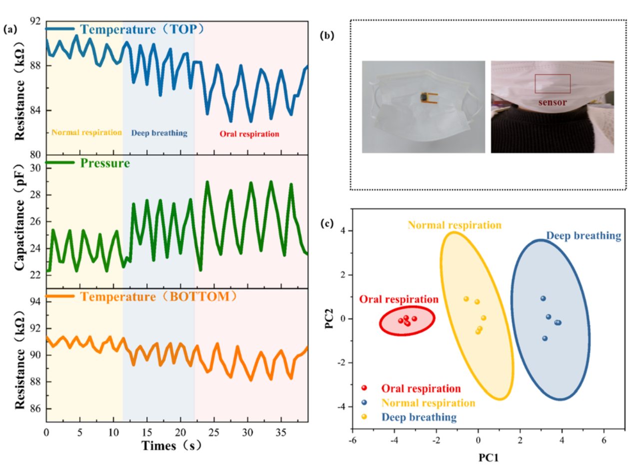

Fig. 15 Application of the e-skin sensor in respiratory monitoring: (a) breath test waveform; (b) schematic diagram; (c) PCA analysis.

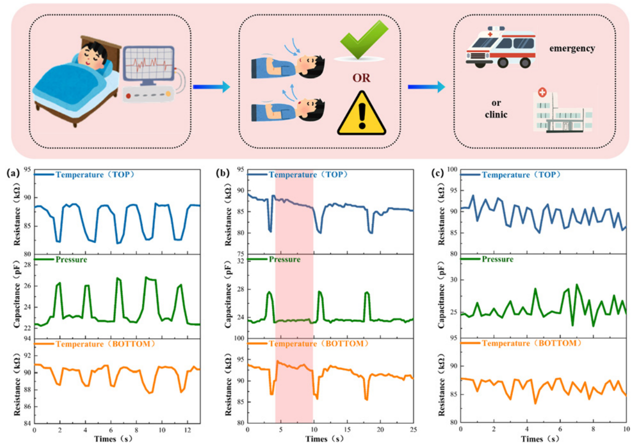

Fig. 16 Sleep monitoring in three states: (a) regular breathing; (b) apnea; (c) rapid breathing.

treatment if necessary. As shown in Fig. 16(a), during normal sleep, users' sleep breathing should show regular changes. However, if a user is experiencing sleep apnea, the sensor can sensitively detect the occurrence of apnea, as indicated by the red area marked in Fig. 16(b). As shown in Fig. 16(c), if the recorded sleep breathing rate increases while the amplitude decreases significantly, it indicates that the user's breathing at that time is too shallow and represents an abnormal breathing pattern. This suggests that the user is experiencing a disturbed sleep state, which may include nightmares. Because the sensor has dual sensitivity to pressure and temperature, it is able to detect both short and high sleep breathing rates. A series of tests confirmed the sensor's significant potential in the field of sleep breathing monitoring.

Conclusions

This study employs an improved electrostatic spinning layered integration process to fabricate a sandwich-structured CNFs/Al_2O_3–SiC SBD pressure–temperature dual-mode e-skin, the top and bottom layers are composed of the temperature-sensitive material SiC SBD, which also functions as capacitive electrodes, forming a capacitive pressure sensor together with the pressure-sensitive material CNFs/Al_2O_3 in the middle layer, which were tested under pressure and temperature conditions. In the pressure test of 5 kPa, the response time of the pressure sensor is 0.52 s, and the recovery time is 0.53 s. In the range of 0–10 kPa, the sensitivity of the pressure sensor can reach 0.366 kPa^{-1}. In the temperature range of 25–50 °C, the response/recovery time of the top layer temperature sensor is 5.12 s/8.97 s. The sensor's sensitivity can reach −1.291 $°C^{-1}$ (25–50 °C), −0.382 $°C^{-1}$ (50–100 °C), and −0.147 $°C^{-1}$ (100–300 °C). In the temperature range of 25–50 °C, the response/recovery time of the bottom layer temperature sensor is 4.96 s/8.92 s. The sensor's sensitivity can reach −1.614 $°C^{-1}$(25–50 °C), −0.382 $°C^{-1}$ (50–100 °C) and −0.157 $°C^{-1}$ (100–300 °C). The CNFs/Al_2O_3–SiC SBD dual-mode e-skin has good repeatability and stable performance after multiple tests. In the test of independent sensing characteristics, the CNFs/Al_2O_3–SiC SBD pressure–temperature dual-mode e-skin can show independent sensing performance, which only responds to specific conditions and is basically not disturbed by other conditions. In addition, the prepared CNFs/Al_2O_3–SiC SBD pressure–temperature dual-mode e-skin can perform human activities such as finger pressing, bending, clapping, swallowing and exhaling, and can detect the spatial distribution of external stimuli, which is suitable for application in intelligent human–machine interfaces and wearable health monitoring devices.

Author contributions

Conceptualization: He Gong, XiuLing Yu, and Ying Guo; writing – original draft preparation: Lingyun Ni; writing – review and editing: He Gong, Lingyun Ni, and Lan Luo; validation: Hongli Chao and Jinfan Wei; formal analysis: Hang Zhu and Mengchao Chen; resources: Zhiqiang Cheng; methodology: Ye Mu and Tianli Hu. All authors have read and agreed to the published version of the manuscript.

Conflicts of interest

There are no conflicts to declare.

Data availability

All relevant data have been presented in charts or tables in the paper.

Acknowledgements

This work was supported by the Science and Technology Department of Jilin Province [grant number: 20230101284JC] and the Department of Education of Jilin Province [grant number: JJKH20240467KJ].

References

1 K. Sedat, O. Ozgür and A. M. Hazar, *et al.*, Flexible capacitive and piezoresistive pressure sensors based on screen-printed parylene C/polyurethane composites in low-pressure range, Flexible and Printed, *Electronics*, 2023, **8**(3), 035015.
2 Z. Tao, Z. Wentao and L. Yang, *et al.*, High-efficient flexible pressure sensor based on nanofibers and carbon nanotubes for artificial electronic skin and human motion monitoring, *J. Porous Mater.*, 2023, **30**(6), 1797–1806.
3 X. Wang, Q. Gao and W. D. Schubert, *et al.*, Review on Electrospun Conductive Polymer Composites Strain Sensors, *Adv. Mater. Technol.*, 2023, **8**(16), 2300293.
4 Z. Kaili, J. WenShuai and L. Xiaokuan, *et al.*, Highly stretchable and sensitive strain sensors based on modified PDMS and hybrid particles of AgNWs/graphene, *Nanotechnology*, 2022, **34**(6), 06LT01.
5 J. Pan, S. Liu and H. Zhang, *et al.*, A Flexible Temperature Sensor Array with Polyaniline/Graphene–Polyvinyl Butyral Thin Film, *Sensors*, 2019, **19**(19), 4105.
6 L. Mengzhuan, Z. Zhongjie and Y. Li, *et al.*, A High-Performance, Sensitive, Wearable Multifunctional Sensor Based on Rubber/CNT for Human Motion and Skin Temperature Detection., *Adv. Mater.*, 2021, **34**(1), e2107309.
7 W. Junjie, W. Nan and X. Da, *et al.*, Flexible humidity sensors composed with electrodes of laser induced graphene and sputtered sensitive films derived from poly(ether-ether-ketone), *Sens. Actuators, B*, 2023, **375**, 132846.
8 W. Wenqing, O. M. N. Goni and W. Haoyang, *et al.*, Gas-Permeable Highly Sensitive Nanomesh Humidity Sensor for Continuous Measurement of Skin Humidity, *Adv. Mater. Technol.*, 2022, **7**(12), 2200479.
9 F. Zheng, Y. H. Jiang and T. X. Yang, *et al.*, Reviews of wearable healthcare systems based on flexible gas sensors, *Chem. Eng. J.*, 2024, **490**, 151874.
10 H. Dong, X. Li and Y. Liu, *et al.*, Ultra-Flexible, Breathable, and Robust PAN/MWCNTs/PANI Nanofiber Networks for High-Performance Wearable Gas Sensor Application., *ACS Sens.*, 2024, **9**(6), 3085–3095.
11 L. Sunghoon, F. Sae and F. H. Arab, *et al.*, Nanomesh pressure sensor for monitoring finger manipulation without sensory interference., *Science*, 2020, **370**(6519), 966–970.
12 G. Xiaohui, Z. Deyi and H. Weiqiang, *et al.*, Biologically Emulated Flexible Sensors With High Sensitivity and Low Hysteresis: Toward Electronic Skin to a Sense of Touch, *Small*, 2022, **18**(32), e2203044.
13 Y. Rui, X. Tiancheng and W. Bang, *et al.*, Highly Sensitive Flexible Piezoresistive Sensor with 3D Conductive Network, *ACS Appl. Mater. Interfaces*, 2020, **12**(31), 35291–35299.
14 B. Liu, Y. Zhou and L. Chen, *et al.*, High-Performance Sensors Based on Chinese Ink and Water-Based Glue for Detection of Strain, Temperature, and Humidity, *ACS Sustainable Chem. Eng.*, 2022, **10**(5), 1847–1856.
15 Q. Feng, C. Zhang and R. Yin, *et al.*, Self-Powered Multifunctional Electronic Skin Based on Carbon Nanotubes/Poly(Dimethylsiloxane) for Health Monitoring, *ACS Appl. Mater. Interfaces*, 2022, **14**, 21406–21417.
16 J. W. Fastier-Wooller, V. T. Dau and T. Dinh, *et al.*, Pressure and temperature sensitive e-skin for in situ robotic applications, *Mater. Des.*, 2021, **208**, 109886.
17 Y. Yiming, W. Yalong and L. Huayang, *et al.*, A flexible dual parameter sensor with hierarchical porous structure for fully decoupled pressure–temperature sensing, *Chem. Eng. J.*, 2022, **430**, 133158.
18 K. Sedat, O. Ozgür and A. M. Hazar, *et al.*, Flexible capacitive and piezoresistive pressure sensors based on screen-printed parylene C/polyurethane composites in low-pressure range, *Flexible Printed Electron.*, 2023, **8**, 035015.
19 Y. Xiong, Y. Zhu and X. Liu, *et al.*, A flexible pressure sensor based on melamine foam capped by copper nanowires and reduced graphene oxide, *Mater. Today Commun.*, 2020, 24100970.

20 C. Lixia, H. Xiaojian and L. Guochang, *et al.*, A Flexible Pressure Sensor Based on Silicon Nanomembrane, *Biosensors*, 2023, **13**(1), 131.
21 B. Sun, G. Xu and X. Ji, *et al.*, A strain-resistant flexible thermistor sensor array based on CNT/MXene hybrid materials for lithium-ion battery and human temperature monitoring, *Sens. Actuators, A*, 2024, 368115059.
22 Y. ZongYao, L. JianYong and N. JiaRong, Research of a Novel Ag Temperature Sensor Based on Fabric Substrate Fabricated by Magnetron Sputtering, *Materials*, 2021, **14**(20), 6014.
23 H. Ronggang, W. Liang and T. Xinling, *et al.*, Facile fabrication of rGO/LIG-based temperature sensor with high sensitivity, *Mater. Lett.*, 2021, **304**, 130637.
24 C. J. Ujam and D. A. Adeniyi, Temperative Dependence of Electrical Conductivity in Semiconductors, *J. Eng. Res. Rep.*, 2021, 30–37.
25 L. Yuan, Z. Wang and Y. Meng, *et al.*, Oxygen doping modulating thermal-activated charge transport of reduced graphene oxide for high performance temperature sensors, *Chin. Chem. Lett.*, 2023, **34**, 108569.
26 O. Y. Kweon, S. J. Lee and J. H. Oh, Wearable High-Performance Pressure Sensors Based on Three-Dimensional Electrospun Conductive Nanofibers, *NPG Asia Mater.*, 2018, **10**(6), 540–551.
27 Z. Han, Z. Cheng and Y. Chen, *et al.*, Fabrication of Highly Pressure-Sensitive, Hydrophobic, and Flexible 3D Carbon Nanofiber Networks by Electrospinning for Human Physiological Signal Monitoring, *Nanoscale*, 2019, **11**(13), 5942–5950.
28 H.-Y. Mi, X. Jing and B. N. Napiwocki, *et al.*, Fabrication of Fibrous Silica Sponges by Self-Assembly Electrospinning and Their Application in Tissue Engineering for Three-Dimensional Tissue Regeneration, *Chem. Eng. J.*, 2018, **331**, 652–662.
29 H. O. Lee, P. H. Caraballa and A. G. Bregman, *et al.*, Fabrication of Tantalum and Hafnium Carbide Fibers via ForcespinningTM for Ultrahigh-Temperature Applications, *Adv. Mater. Sci. Eng.*, 2021, **2021**(1), 6672746.
30 Z. Jizhen, K. Na and U. Simge, *et al.*, Scalable Manufacturing of Free-Standing, Strong $Ti_3C_2T_x$ MXene Films with Outstanding Conductivity., *Adv. Mater.*, 2020, **32**(23), e2001093.
31 A. Lipatov, H. Lu and M. Alhabeb, *et al.*, Elastic properties of 2D $Ti_3C_2T_x$ MXene monolayers and bilayers, *Sci. Adv.*, 2018, **4**(6), eaat0491–eaat0491.
32 F. Wenjing, L. Cheng and L. Wei, *et al.*, 3D Waterproof MXene-Based Textile Electronics for Physiology and Motion Signals Monitoring, *Adv. Mater. Interfaces*, 2022, **9**(14), 2102553.
33 Y. Fan, H. Zhao and F. Wei, *et al.*, A facile and cost-effective approach to fabrication of high performance pressure sensor based on graphene-textile network structure, *Prog. Nat. Sci.: Mater. Int.*, 2020, **30**(3), 437–442.
34 A. Jingwen, W. Qingqing and L. Zhuquan, *et al.*, Highly Stretchable and Fluorescent Visualizable Thermoplastic Polyurethane/Tetraphenylethylene Plied Yarn Strain Sensor with Heterogeneous and Cracked Structure for Human Health Monitoring., *ACS Appl. Mater. Interfaces*, 2024, **16**(1), 1428–1438.
35 G. Changshun, Q. Wenjing and W. Yanli, *et al.*, Highly stretchable, durable, and superfine fiber-shaped strain sensor with a porous core-sheath microstructure, *Compos. Commun.*, 2022, **36**, 101381.
36 G. Bellocchi, M. Vivona and C. Bongiorno, *et al.*, Barrier height tuning in Ti/4H-SiC Schottky diodes, *Solid State Electrochem.*, 2021, **186**, 108042.
37 S. Min, C. M. Shin and T. N. Nguyen, *et al.*, High-Performance Temperature Sensors Based on Dual 4H-SiC JBS and SBD Devices, *Materials*, 2020, **13**(2), 445.
38 I. Capan, R. Bernat, T. Makino and T. Knežević, 4H-SiC Schottky Barrier Diodes as Radiation Detectors: A Role of Schottky Contact Area, *Diamond Relat. Mater.*, 2023, **137**, 110072.
39 C. Mu, Y. Song and W. Huang, *et al.*, Flexible Normal-Tangential Force Sensor with Opposite Resistance Responding for Highly Sensitive Artificial Skin, *Adv. Funct. Mater.*, 2018, **28**(18), 1707503.
40 B. Boyarbay, H. Çetin, M. Kaya and E. Ayyildiz, Correlation between Barrier Heights and Ideality Factors of H-Terminated Sn/p-Si(100) Schottky Barrier Diodes, *Microelectron Eng.*, 2008, **85**(4), 721–726.